Measurements and Physics-Based Analysis of Co-Located Antenna Pattern Diversity System

Fikadu T. Dagefu, Jungsuek Oh, *Member, IEEE*, Jihun Choi, *Student Member, IEEE*, and Kamal Sarabandi, *Fellow, IEEE*

***Abstract*—This paper investigates the advantages offered by radiation pattern diversity using a new physics-based analysis that takes into account the complex radiation patterns of the transmit(Tx) and receive(Rx) diversity antennas in conjunction with an accurate deterministic, coherent, and polarization preserving propagation model for a complex indoor scenario. Unlike techniques that utilize spatial diversity, radiation pattern diversity offers a unique opportunity to achieve compact diversity antenna systems especially with the advent of enabling antenna miniaturization techniques. In this work, a co-located antenna radiation pattern diversity system is proposed and its performance is analyzed using an accurate physics-based diversity analysis technique. The proposed analysis technique utilizes an efficient deterministic propagation model modified by incorporating the complex gain of the Tx and the complex effective heights of the Rx antennas into the rays launched and received by the antennas in a coherent manner. The proposed system is realized and tested in complex indoor scenarios based on which complex correlation coefficients between various channels and the effective diversity gain are computed which are then utilized as a figure of merit for improved channel reliability. For the scenarios considered, it is shown that the apparent diversity gain is at least 9.4 dB based on measured results.**

***Index Terms*—Antenna pattern diversity, co-located antennas, diversity analysis, near-ground propagation.**

I. Introduction

An aspect of wireless communication that is of paramount importance is reliable connectivity unhampered by signal fading caused by scatterers such as walls, buildings and other obstacles. For power limited ad hoc networks in complex environments such as indoor and urban environments, various phenomena including multipath, diffraction from sharp corners and edges and scattering from other obstacles contribute to the fading and distortion of electromagnetic waves that severely limit the coverage and reliability. The signal that arrives at a receiver operating in such environment is the sum of the direct path between Tx and Rx antennas attenuated by penetrable objects as well as signal components scattered by indoor obstacles. Because of the difference in path length among the various signal components and in the absence of a direct signal, the received electric field will have uneven spatial distribution and significant fluctuations. This phenomenon is called fast fading and results in intermittent signal drop-offs causing the communication channel to be unreliable. A viable approach to mitigate fast fading is the use of antenna diversity systems. Antenna Diversity is a communication method utilizing multiple antennas to receive and/or transmit signals to capture statistically independent copies of the signal to compensate for the multipath interferences. Diversity systems enable improvement in signal-to-noise-ratio (SNR) without increasing the transmit power.

In the literature, there are five different types of diversity techniques that can be used to improve channel reliability: spatial, temporal, polarization, frequency, and radiation pattern. Of these, only spatial, polarization and pattern make for a practical implementation in WLAN antenna systems. In [1], an analysis of a spatial diversity system based on simulations and measurements is presented. The performance of a dual-antenna handset for which different antenna types were utilized is investigated with particular focus on industrial, scientific, and medical (ISM) band [2]. In [3], a test system to experimentally determine the complex correlation coefficient between two antenna branches is proposed and was utilized to evaluate the polarization diversity performance of different antenna pairs in Rayleigh and Rician distributions which are often used to model indoor environments. In [4], experiments where antenna separation, polarization, and pattern were varied independently were carried out and the performance of the diversity system is analyzed. Other researchers have also reported analysis results of various diversity systems based on measurement and stochastic indoor propagation models [5]–[8]. For small wireless devices, spatial diversity scheme is not an option due to limited space on such devices. In a rich multipath environment where signal fading is strong and signal's direction of arrival to the receiver is diverse, radiation pattern diversity is most suitable. Pattern diversity often refers to antenna systems composed of two or more arrays with beams pointing in different directions to collect statistically independent rays arriving from different directions. Again for small wireless platforms such solution is not appropriate. Small common aperture antennas with multiple feeds that can produce almost orthogonal radiation patterns are envisioned for these applications [9], [10].

Manuscript received December 08, 2012; revised July 01, 2013; accepted July 30, 2013. Date of publication August 15, 2013; date of current version October 28, 2013. This work was supported in part by the U.S. Army Research Laboratory under contract W911NF and prepared through collaborative participation in the Microelectronics Center of Micro Autonomous Systems and Technology (MAST) Collaborative Technology Alliance (CTA) and NSF under contract ECCS 1101868.

The authors are with the Radiation Laboratory, Department of Electrical Engineering and Computer Science, The University of Michigan, Ann Arbor, MI 48109 USA (e-mail: fikadu@umich.edu; jungsuek@umich.edu; jihchoi@umich.edu; saraband@umich.edu).

Color versions of one or more of the figures in this paper are available online at http://ieeexplore.ieee.org.

Digital Object Identifier 10.1109/TAP.2013.2277913

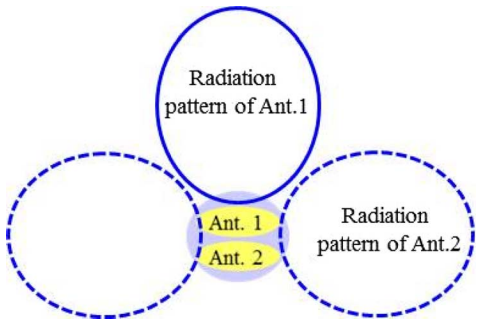

Fig. 1. Schematic of a radiation pattern diversity using two antennas having omnidirectional and broadside radiation patterns, respectively.

A thorough and accurate analysis of a diversity system needs three main components: the Tx and Rx antenna radiation patterns (phase and amplitude), the multipath coherent propagation model and the calculation of a figure of merit for the performance of the diversity system such as complex and envelop correlation coefficients and/or diversity gain. Existing simulation based diversity analysis techniques especially from the communication system society model the indoor or other multipath channel using a stochastic model such as Rayleigh and Rician distributions. While these probabilistic models provide generalized approximations to the indoor channel, such models do not accurately capture all the propagation mechanisms such as angle of arrival and polarization, and hence diversity analysis techniques based on such models inherently lack the information needed to assess the true performance of a given diversity system. For example, for near-ground antennas, propagation supported by Norton surface waves have to be captured for accurate field calculations. Specifically, for Tx and Rx antennas located less than a wavelength (λ) above ground, wave propagation is dominated by Norton surface waves [11], [12]. The other aspect of diversity system is the design of a common aperture radiation pattern diversity antenna. Recently, different types of antenna topologies with radiation pattern diversity have been reported [13], [14]. In such literature, one antenna has omnidirectional radiation pattern, and the other antenna has broadside radiation pattern, as depicted in Fig. 1. While the antenna geometries in the literature provide the desirable isolation between two antennas, they are based on multi-layer structures, that cannot be easily fabricated and are not easily amenable to miniaturization. This paper introduces a new approach to design an antenna with a small form factor and co-polarized radiation pattern diversity.

In this paper, we discuss a new diversity system analysis approach that takes into account the complex radiation pattern of the Tx and Rx diversity antennas and make use of an accurate deterministic, coherent, and polarization preserving propagation model for a complex indoor scenario. One advantage of this approach is that for a diversity system deployed in complex scenarios the performance can be quantified accurately since all the propagation mechanisms are accounted for. In Section II, the new physics-based pattern diversity analysis approach will be introduced. The propagation modeling with specific focus on near-ground antennas will also be discussed. An accurate near-ground indoor propagation model that can accurately capture scattered field components from indoor obstacles while fully taking into account the Norton surface waves will be discussed as well. An example analysis of a near-ground diversity system based on this model will also be presented. In Section III, the design of a co-located radiation pattern diversity antenna will be described which is used in a pattern diversity measurement system. Finally, in Section IV, the diversity measurement system to measure the amplitude and phase of the received field needed for computing the complex correlation coefficients will be presented.

II. Physics-Based Simulation and Analysis of Pattern Diversity Systems

As it was alluded to in the previous section, the objective of this section is to discuss a new approach to analyze the performance of a diversity system. This technique will be utilized to investigate the performance of the pattern diversity system based on a common aperture pattern diversity antenna described in Section III. Of the various diversity techniques mentioned in the previous section, for small platforms, spatial diversity is not possible. However, it is possible to use a small antenna with two or more feeds to generate different radiation patterns. The main idea of pattern diversity approach is to utilize antenna systems with different ports that radiate electromagnetic fields in mutually exclusive (almost) directions and when positioned in multipath environments can receive the fields in mutually exclusive directions. This results in simultaneous field measurements that are statistically uncorrelated and thus can be utilized to improve the wireless connectivity.

The block diagram in Fig. 3 shows the proposed diversity analysis technique. In this section, the steps for calculating the open circuit voltage (V_{oc}) at the Rx ports and the complex correlation coefficients between the various channels is described. We will then discuss two sets of results: 1) a near-ground scenario where the antennas are within a wavelength above ground, and 2) a case where the antenna heights are greater than a wavelength. At the frequency of operation used for this analysis (400 MHz), if the antenna heights are above λ (75 cm), the ray-tracing approach is a good approximation. For the near-ground case, we will utilize an efficient propagation model that we developed for this application.

A. Calculation of Rx Open Circuit Voltage and Complex Correlation Coefficients

Here, we will discuss the steps required to calculate the complex correlation coefficients between the different channels (e.g., the horizontal and vertical pattern channels as illustrated in Fig. 2). First, the complex radiation pattern of the Tx antenna system for all directions, i.e., the complex normalized electric field values (in the far-field) computed as a function of θ and ϕ, are imported. For each value of θ and ϕ, rays are launched by taking into account the complex pattern data in that direction. All the rays are then used as sources to illuminate the multipath propagation environment in which the antennas are operating. For each Tx-Rx arrangement, an accurate deterministic propagation model is used to calculate the electric field incident on each Rx antenna element as a function of θ and ϕ (these angles

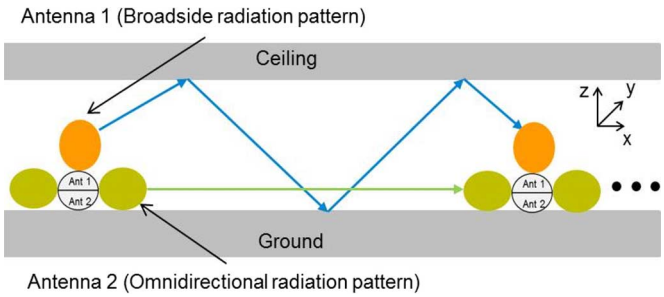

Fig. 2. Schematic of a radiation pattern diversity system in a hallway (side view) environment.

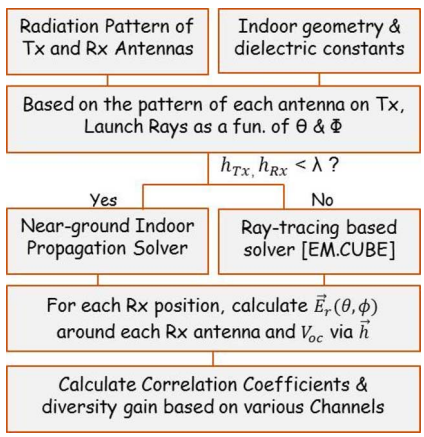

Fig. 3. Diagram of the proposed physics-based diversity system analysis approach, $E_r(\theta,\phi)$, V_{oc} and $\vec{h}$ are received field, open circuit at the Rx channel and antenna effective height, respectively. h_{Tx} and h_{Rx} are the heights of the Tx and Rx antennas.

are with respect to the location of the Rx antenna). The real and imaginary parts of the incident electric field in conjunction with the effective Rx antenna height is used to calculate the open circuit voltage at each Rx antenna port.

The effective height of the antenna $(\vec{h})$ can be expressed in terms of a matched load Z_L, the complex pattern of the Rx antenna $(G(\theta,\phi))$, the complex polarization vector of the Rx antenna $(\vec{p})$, free space impedance (Z_o), and the wavelength (λ) as

$$\vec{h}(\theta,\phi) = \sqrt{\frac{Z_L\lambda^2 G(\theta,\phi)\Gamma}{Z_o\pi}}\vec{p^r}. \tag{1}$$

The polarization matching factor (Γ) and the intermediate variables (a, b, β and α) based on the definition given in [15] are given by

$$\frac{p^i_\theta}{p^i_\phi} = a\,e^{j\alpha} \;\&\; \frac{p^r_\theta}{p^r_\phi} = b\,e^{j\beta} \tag{2}$$

$$\Gamma = \frac{1+2ab\,cos(\alpha+\beta)+a^2b^2}{(1+a^2)(1+b^2)} \tag{3}$$

where $p^i_{\theta,\phi}$ and $p^r_{\theta,\phi}$ are the components of the polarization vectors of the incident field and the receive antenna, respectively.

We can then calculate the open circuit voltage (V_{oc}) by including the polarization mismatch factor as

$$V_{oc} = \vec{E^i}(\theta,\phi)\cdot\vec{h}(\theta,\phi) = \vec{E^i}(\theta,\phi)\cdot\sqrt{\frac{Z_L\lambda^2 G(\theta,\phi)\Gamma}{Z_o\pi}}\vec{p^r} \tag{4}$$

where $\vec{E^i}$ is the complex received electric field at the location of receive antenna element. Finally, if v_1 and v_2 are the open circuit voltages at the two ports of the receive antennas, the complex correlation coefficient between the two channels can be computed using

$$\rho_c = \frac{\langle v_1 v_2^*\rangle - \langle v_1\rangle\langle v_2^*\rangle}{\sqrt{(\langle|v_1|^2\rangle - |\langle v_1\rangle|^2)(\langle|v_2|^2\rangle - |\langle v_2\rangle|^2)}} \tag{5}$$

where $\langle\cdot\rangle$ represents the expected value operator calculated using the spatial samples of v_1 and v_2.

Another parameter commonly used to quantify the effectiveness of a given diversity system is diversity gain. Apparent diversity gain is the ratio between the received SNR of the combined signal and that of the best branch for a given outage rate (given by the corresponding CDF curves) [16]. In this paper, the diversity gain is calculated by using a selection combining criteria with maximum apparent diversity gain of 10.48 and an outage rate of 1% [17]–[19]. As described in [20], the apparent Diversity Gain(ADG) is given by

$$ADG = 10.48\sqrt{1-|\rho_c|^2}. \tag{6}$$

B. Simulation Result of the Pattern Diversity Antenna in a Complex Indoor Scenario

In this section the performance characteristics of the proposed co-located pattern diversity antenna system is studied through simulation of wave propagation in a complex multipath indoor environment. A two story office building shown in Fig. 4 is used for analyzing the performance of the proposed system. Two different propagation solvers are utilized. The first set of results presented in this section is based on a commercial ray-tracing based propagation solver called EM.CUBE [20]. In the next section a propagation model that we developed to analyze near-ground diversity systems is utilized. The building structure consists of several rooms where the walls are modeled as lossy dielectric slabs having a thickness of 50 cm. The dielectric properties of the walls is assumed to be that of a brick wall ($\epsilon_r = 4.4$ and $\sigma = 0.004$). The Tx and Rx pattern diversity antennas used for this simulation are co-located monopole and compact bowtie patch antennas. A detailed description is included in the next section. The complex building structure shown in Fig. 4(a) is modeled using EM.CUBE and for each radiating elements of the Tx pattern diversity antenna data are imported. For each new Rx position, the electric field corresponding to rays that are incident on the Rx antenna are calculated as a function of θ and ϕ. The incident electric field is exported and is used to compute the open circuit voltage at each

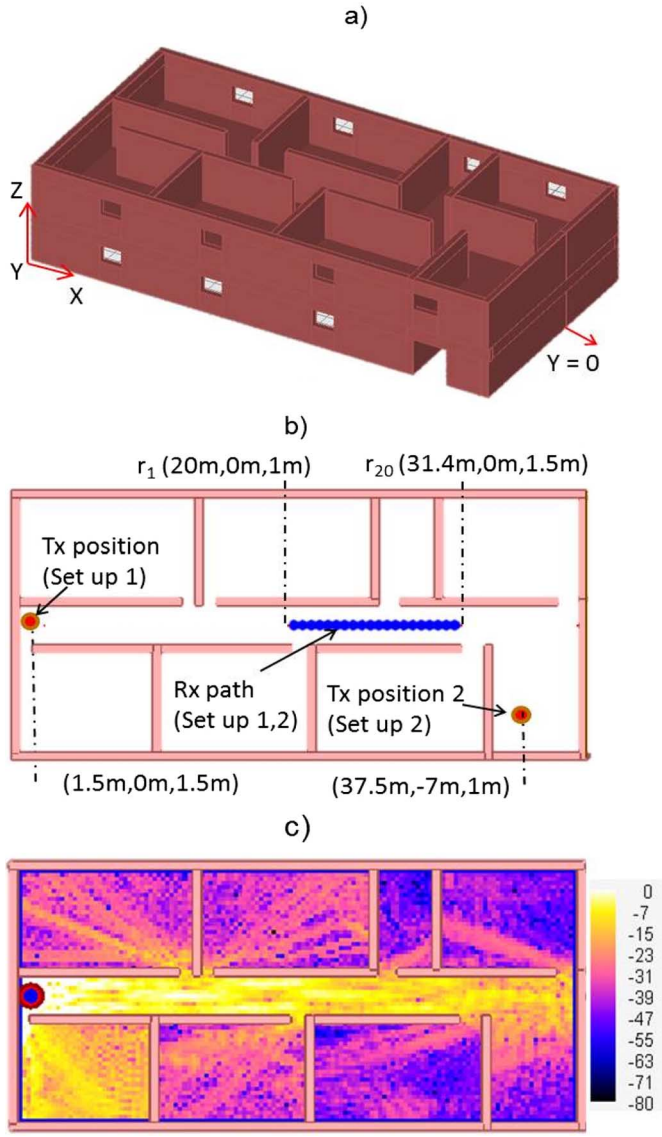

Fig. 4. (a) Simulation geometry (ceiling and ground not shown but are included in the simulation), (b) the top view and the Tx-Rx configurations for diversity system simulation analysis, and (c) signal coverage when Tx is at Position 1 on a plane parallel to the ground at 1-m height.

Rx ports based on the effective antenna heights of the Rx antenna elements.

In the first case of the simulation of the diversity system, the Tx and Rx antennas are deployed along the corridor on the first floor of the building where the location of the Rx antenna is changed along Rx path as shown in Fig. 4(b), and the transmitter is located at Tx position 1. This case is chosen to analyze the performance of the diversity system when there is a line of sight (LoS) between the Tx and Rx antennas. By following the procedure described above, the open circuit voltages at the Rx antenna elements are computed. As can be seen in Fig. 5, the V_{oc} curves show the uncorrelated variation of the various channels. In Fig. 5(a), the monopole is used as the Tx antenna and the two curves show the channels created when the monopole and patch antennas are used as a Rx antennas. For this scenario (LoS case), the vertical channel is mainly supported by the rays that bounce back and forth between the ground and the ceiling.

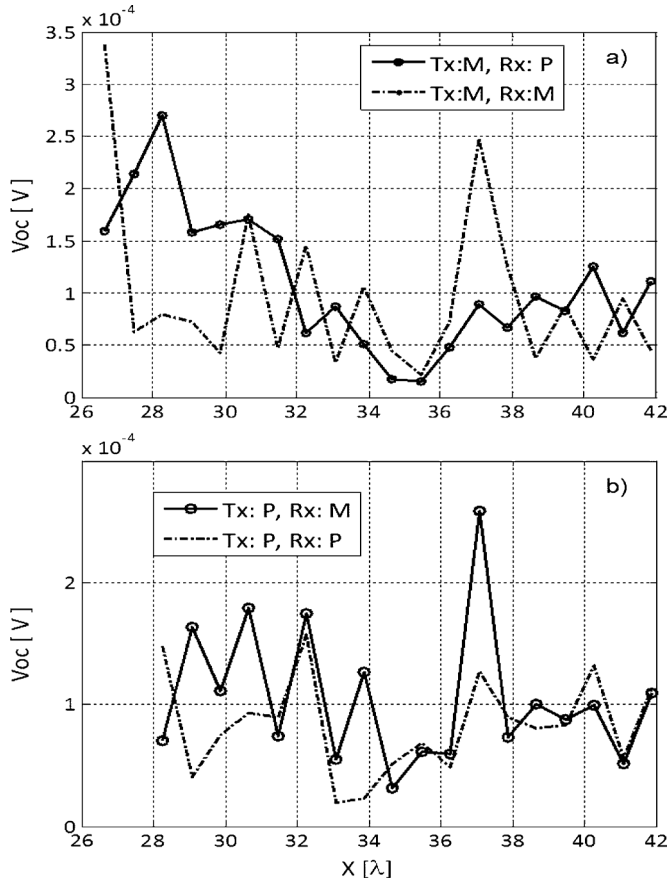

Fig. 5. Computed open circuit voltage values at the outputs of a radiation diversity antenna composed of co-located patch and monopole antenna (a) when monopole antenna is transmitting and (b) when the patch antenna is transmitting.

The horizontal channel is mostly from multiple reflections from the side walls.

A case where there is no line of sight between the Tx and Rx antennas as shown in Fig. 4(b) is also simulated (Tx position 2 and Rx path). In this case the received fields are mainly supported by the walls, ground and ceiling of the center hallway similar to the LoS case, but instead of the direct path, edge diffraction and penetration through walls also contribute to the NLoS case.

C. Near-Ground Propagation Modeling and Analysis

For near-ground transceivers deployed in multipath environments, electromagnetic wave propagation is dominated by Norton surface waves. In order to accurately calculate electric field coverage in complex propagation scenarios such as indoor environments, these higher order waves and their interactions with building walls and other indoor obstacles have to be captured. Full-wave solutions are computationally inefficient for indoor propagation simulations. The most commonly used field prediction techniques are based on ray tracing routines which are based on geometrical optics (GO). Ray tracing approaches are inadequate for evaluating signal coverage of transceiver nodes very close to the ground (less than a wavelength above ground) since such routines neglect higher order surface waves. For this reason we need to devise a technique that can efficiently capture the higher order surface waves and their

interactions with the obstacles. Our approach for calculation of near-ground wave propagation and scattering is based on a physical optics solution where an asymptotic approximation of the Dyadic Green's function for a half-space dielectric medium is utilized. In our recent work, we developed a near-ground indoor propagation approach that fully takes into account the higher order Norton surface waves [12]. The field components scattered from indoor obstacles such as walls are computed using a physical optics approximation in conjunction with an efficient solution of the half-space Dyadic Green's function.

In this work, we extended this model to make it more efficient by taking into account the dominant scattering mechanisms when calculating scattering from indoor obstacles. The modified approach is implemented for hallway geometry similar to Fig. 2. Essentially, the geometry consists of the ground, ceiling and two side walls as shown in Fig. 2. When a radiation pattern diversity antenna (will be described in the next section) having two radiating elements as depicted in Fig. 1 is positioned in one end of this hallway very close to the ground, there will be a vertical and horizontal channel that are supported. The proposed propagation technique calculates the direct path between Tx and Rx, by radiating the current distribution on the Tx antenna using the Dyadic Green's function for a half-space medium discussed above. The first order reflections and multiple scattering from side walls are calculated based on the image method. In all the calculations, the surface waves are included. The open circuit voltage for each channel (when Rx antenna is Monopole or Patch) are calculated following the procedure described in the previous section. The resulting correlation coefficient is less than 0.1.

III. Radiation Pattern Diversity Antenna Design

This section shows the design of a common aperture antenna in a small space having radiation patterns that are significantly different and almost orthogonal. This difference is measured by the envelop cross-correlation (ρ_e) between the radiation patterns in the far-field. This can be done numerically if the theoretical radiation patterns ($\vec{G}(\theta,\phi)$) of both antennas are known in all directions based on

$$\rho_e = \frac{|\iint \vec{G_1}(\theta,\phi) \bullet \vec{G_2}(\theta,\phi) d\Omega|^2}{\iint |\vec{G_1}(\theta,\phi)|^2 d\Omega \iint |\vec{G_2}(\theta,\phi)|^2 d\Omega} \tag{7}$$

where $\bullet$ represents the Hermitian product. Also, $\vec{G_1}(\theta,\phi)$ and $\vec{G_2}(\theta,\phi)$ are radiation patterns of antenna 1 and 2. In practice, it is difficult to know the radiation patterns for arbitrary antennas. To calculate the envelop correlation in this case, a relation between radiation patterns and scattering matrix (S-matrix) has been established [21] and is given by

$$\rho_e = \frac{|S_{11}^* S_{12} + S_{21}^* S_{22}|^2}{((1-(|S_{11}|^2+|S_{21}|^2))(1-(|S_{22}|^2+|S_{12}|^2))}. \tag{8}$$

The above formula assumes uniformly distributed radio channel and lossless antennas [17]. Based on [18] and the efficiency values in Fig. 8, since the total efficiency of the proposed antenna is high over the operating impedance bandwidth, the effect of the losses on the diversity performance is assumed to be small. The proposed antenna system consists of two radiating elements: one with omnidirectional radiation pattern in horizontal plane and the other one with a radiation pattern mainly in the broadside direction as depicted in Fig. 1. It should also be noted that the proposed antenna is a single-mode antenna which is required to justify the use of (8). Fig. 2 shows a simple geometry where the proposed antenna could be used to produce two channels with relatively small correlation. To realize the omnidirectional radiation pattern, a $\lambda/4$ monopole antenna is chosen. The second antenna, which needs to have a broadside radiation pattern was chosen to be a bow-tie patch. By using this antenna, the area of the patch can be reduced by more than 60%, compared to a conventional $\lambda/2$ microstrip antenna. This results in reducing the total dimension of the proposed diversity antenna. In order to make the two antennas co-located in a small space, the monopole antenna is placed in the middle of the bow-tie patch antenna fed by a co-axial line with the outer connector of the co-axial line connected to the bow-tie patch. This enables high isolation between the two antenna feeds since electric potentials are zero in the middle of the bow-tie patch antenna and at the bottom of the monopole antenna.

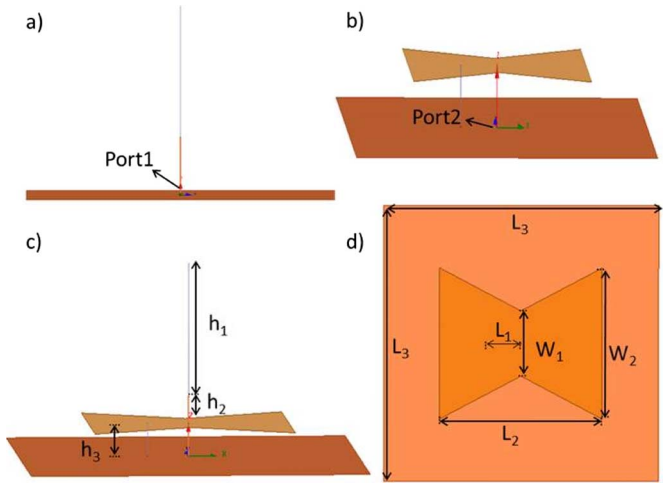

Fig. 6. Geometry and design parameters of the proposed radiation pattern diversity antenna: (a) Monopole antenna, (b) bow-tie patch antenna, (c) proposed radiation pattern diversity antenna, and (d) top-view of the proposed antenna.

The resulting envelope correlation between the two different radiation patterns from the proposed antenna system is quite small. In addition, considering the difficulty of impedance matching of the monopole antenna with stacked ground plane (bow-tie patch and its ground plane), the concept of the sleeve, which is a well-known technique for improving bandwidth and obtaining impedance matching, is applied [23]. In this geometry, a short section (h_2 in Fig. 6) of the coaxial cable protruding over the bow-tie patch antenna acts as an impedance transformer. Also, the bow-tie patch antenna is designed on the air substrate to obtain low dielectric loss. Since the geometry of the bow-tie patch antenna is symmetric in terms of XZ and YZ planes, omnidirectional radiation pattern of the $\lambda/4$ monopole antenna is preserved. Through a parametric study using a full-wave simulator, Ansoft HFSS 13.0, the two operating frequencies of the two antennas are designed to be same.

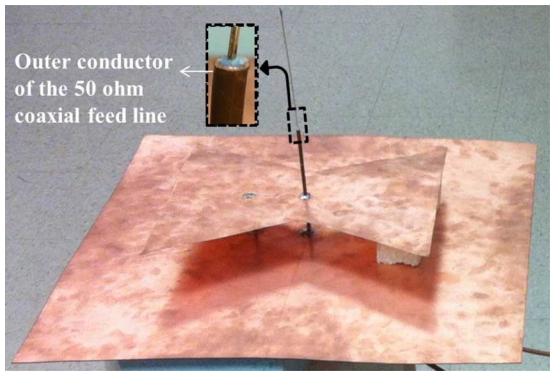

Fig. 7. Proposed pattern diversity antenna designed and fabricated for the 400-MHz diversity system.

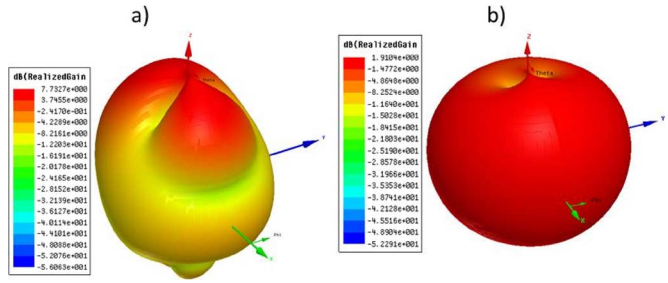

Fig. 9. 3-D radiation patterns (E_θ) of the proposed radiation pattern diversity antenna: (a) when the bowtie patch antenna is transmitting and the $\lambda/4$ monopole antenna is matched with 50 Ohm (broadside radiation pattern), and (b) when the bowtie patch antenna is matched with 50 Ohm and the $\lambda/4$ monopole antenna is transmitting (omnidirectional radiation pattern).

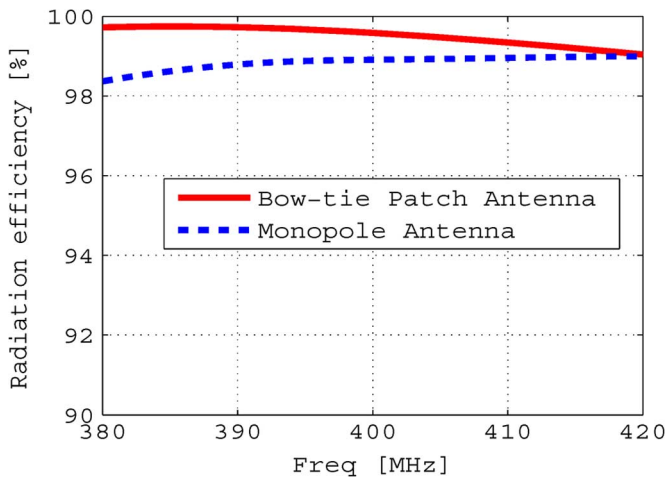

Fig. 8. Simulated radiation efficiency of the two antenna elements in the proposed common aperture co-polarized radiation pattern diversity antenna system.

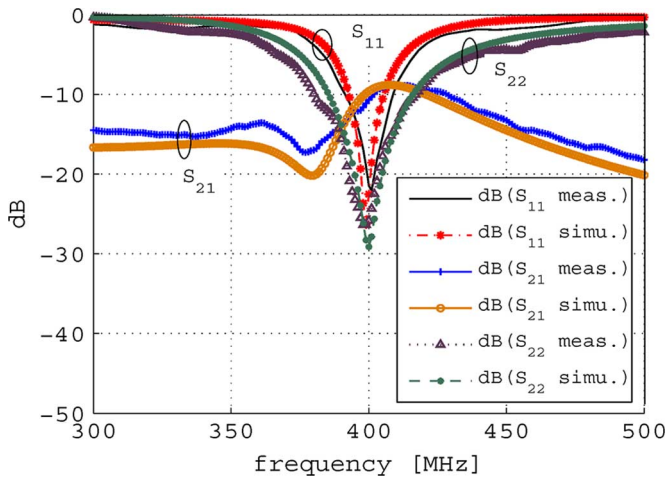

Fig. 10. Measured and simulated S-parameters of the proposed pattern diversity antenna.

Design parameters are shown in Fig. 6. The values are given by L1 = 55 mm, L2 = 270 mm, L3 = 457 mm, W1 = 108 mm, W2 = 250 mm, h1 = 159.5 mm, h2 = 31.5 mm, and h3 = 40 mm. In order to consider ohmic loss, conductivity of copper is used in all metallic traces in the full-wave analysis. Fig. 9 shows the 3-D radiation patterns of the proposed antenna at 400 MHz. The radiation patterns are calculated by exciting one antenna while the other antenna is terminated with 50 Ohm and vice versa. It should be noted that the bow-tie shape and the small ground plane which has a dimension of 0.6λ causes the broader beam of the patch antenna compared to a half-wave microstrip antenna. Based on the simulated design parameters, the pattern diversity antenna is fabricated and measured, as shown in Fig. 7. As can be seen in Fig. 10, the measured S-parameters show good agreement with the simulated S-parameters. It should be noted that (7) is a fundamental definition for the envelop correlation. But, for component level diversity performance analysis, (8) which is the conventional approach as described in [17]–[19], can be used. Phase and amplitude information of the S-parameters are used to calculate the envelop correlation (ρ_e) between the two different radiation patterns. The value of the calculated envelope correlation based on simulated results is shown to be as low as 0.0002 or -37 dB at 400 MHz. Based on the measured data, the value of the envelope correlation is found to be as low as 0.0013 or -29 dB at 400 MHz. The difference between simulated and measured envelope correlation values is due to the cable effects which can affect the radiation performances of the antennas, leading to the slight increase in the interaction between two feeds. Furthermore, inaccuracies in the fabrication of the monopole antenna (which is not strictly perpendicular to the ground plane) cause increased coupling between the two antennas. It should also be noted that the envelop correlation was calculated based on (7) and the HFSS pattern data which came out to be 0.0592. The discrepancy with the result from (7) is caused by assumptions made when (8) is derived [22].

IV. Radiation Pattern Diversity Measurement System and Results

A. System Configuration

In order to investigate indoor wave propagation of radiated fields from the proposed diversity antennas, a system that can accurately measure the amplitude and phase of the received signal is designed and fabricated at 400 MHz. The operating frequency of 400 MHz is chosen considering the allowable size of the antenna and characteristics of indoor wave propagation as

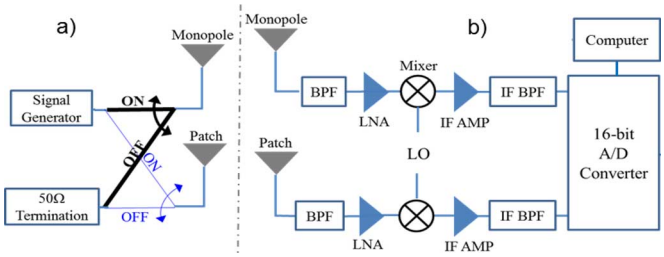

Fig. 11. Schematics of (a) the transmitter and (b) receiver utilizing the proposed diversity antennas.

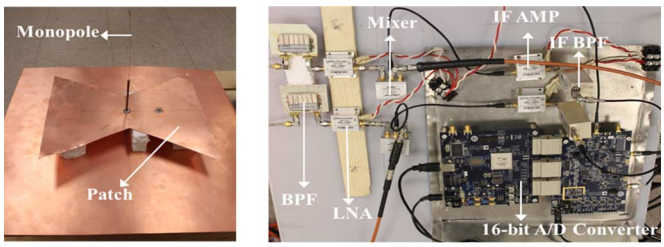

Fig. 12. Photographs of (a) fabricated diversity antenna and (b) receiving module.

a function of the operating frequency. Fig. 11 shows schematics of a transmitter and a receiver utilizing the proposed diversity antenna. When one Tx antenna is connected to a signal generator (ON), the other is terminated to 50 Ohm (OFF). Received signals at both receiving antennas are recorded. In other words, while only one transmitting channel is 'ON', signals at both intended and unintended receiving channels are recorded. By calculating the correlation between the two signals received from two different antennas, the ability of the proposed diversity system to increase channel capacity is evaluated. In the receiver, the received 400 MHz signals are down converted to 20 MHz and the signals are sampled by a highly sensitive 16-bit, 2-channel A/D converter. Since the A/D has a maximum available sampling rate of 80 Mbps, the signal was down-converted to 20 MHz. With this receiver set up, the received data can be easily compared to each other and processed to calculate the correlation. Bandpass filters (BPF) are used to get rid of outer noise signals. Also low noise amplifiers (LNA) and IF amplifiers are used to satisfy the detectable sensitivity of the A/D converters. Also, before carrying out the measurements, we have characterized the Rx channels by directly connecting the BPF (Fig. 11) to signal generator to make sure the two channels provide similar attenuation and phase variations. Fig. 12 shows the photographs of the fabricated antennas and receiving module. In order to realize a channel established by near-ground wave propagation, the diversity antennas are positioned near the ground, about 10 cm (0.13λ at 400 MHz) above the ground.

B. Measurement in Complex Indoor Scenarios

Using the measurement system discussed in the previous section, the propagation measurements are performed in a complex rich multipath indoor environment. Fig. 13 shows the floor plan of the 3rd floor in Electrical Engineering building at the

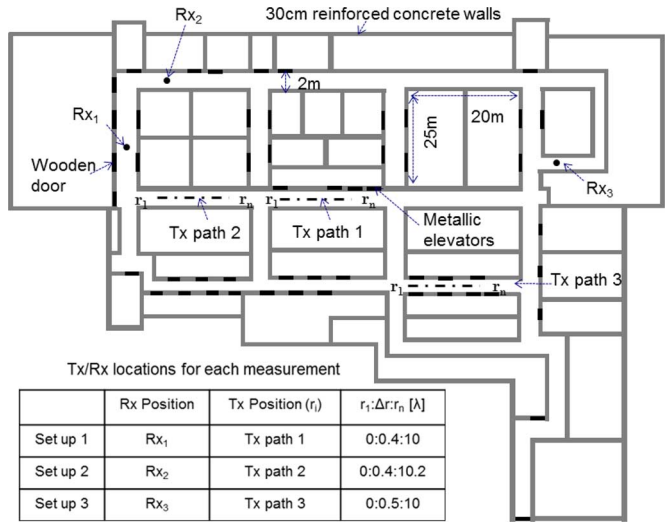

Tx/Rx locations for each measurement

	Rx Position	Tx Position (r_1)	r_1:Δr:r_n [λ]
Set up 1	Rx_1	Tx path 1	0:0.4:10
Set up 2	Rx_2	Tx path 2	0:0.4:10.2
Set up 3	Rx_3	Tx path 3	0:0.5:10

Fig. 13. Floor plan of the Electrical Engineering building at the University of Michigan where the measurements were carried out. A table listing the Tx and Rx positions for each measurement scenario is also included (r_1, r_n are the starting and ending points of each Tx path and Δr is the difference between consecutive Tx positions).

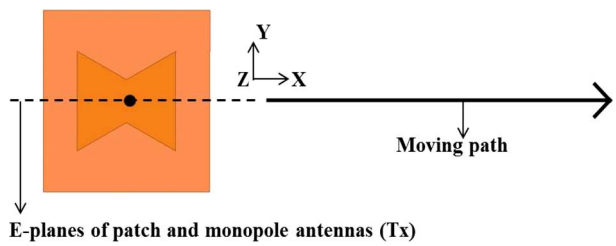

Fig. 14. Schematic showing the E-planes of both antenna elements for the moving Tx antenna.

University of Michigan where the measurement was carried out. The measurement environment consists of several concrete walls and wooden/metallic objects including doors and ceilings. Three different sets of measurements were performed by varying Tx and Rx arrangements. These scenarios were selected in order to assess the performance of the diversity system for different levels of multipath. The positions of the Tx and Rx antennas are given in Fig. 13. In each case the position of the receiver system is fixed and the Tx antenna is moved along the path shown. As noted before, the diversity system has a common aperture co-polarized two-element antenna system. As the Tx antenna is moved along a path (Fig. 14), the polarizations of both antennas are kept as E_θ when the antennas' broadside direction is defined to be along the Z-axis. The magnitude and the phase of the received signal corresponding to each channel is then recorded as a function of the position of the Tx antenna. For each measurement scenario, the received signals which can be considered as complex random variables in terms of the position of the transmitter. For example, v_{PM} is the signal measured when the Tx antenna is the monopole antenna while the Rx is the patch antenna. Finally, the complex correlation coefficient is calculated using (5) based on 25 measurement samples.

The magnitudes of the signals for the first measurement scenario are given in Fig. 15. The output signals from the two Rx antennas (monopole and patch) when the Monopole antenna is

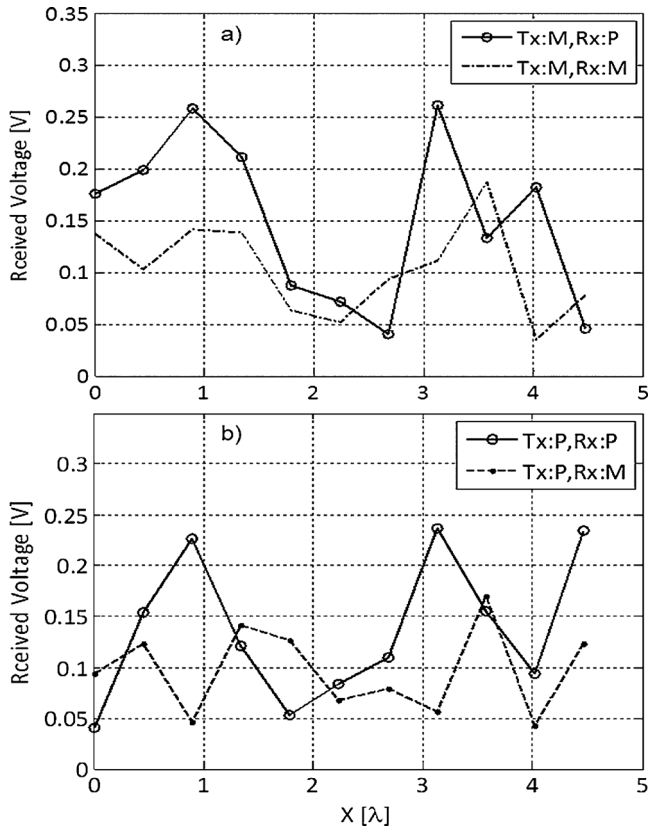

Fig. 15. Measured signals for set up 1 (Fig. 13): (a) when monopole antenna is transmitting while the patch component of the Tx antenna is terminated with 50 Ohm and (b) when the patch antenna is transmitting while the monopole component of the Tx antenna is terminated with 50 Ohm.

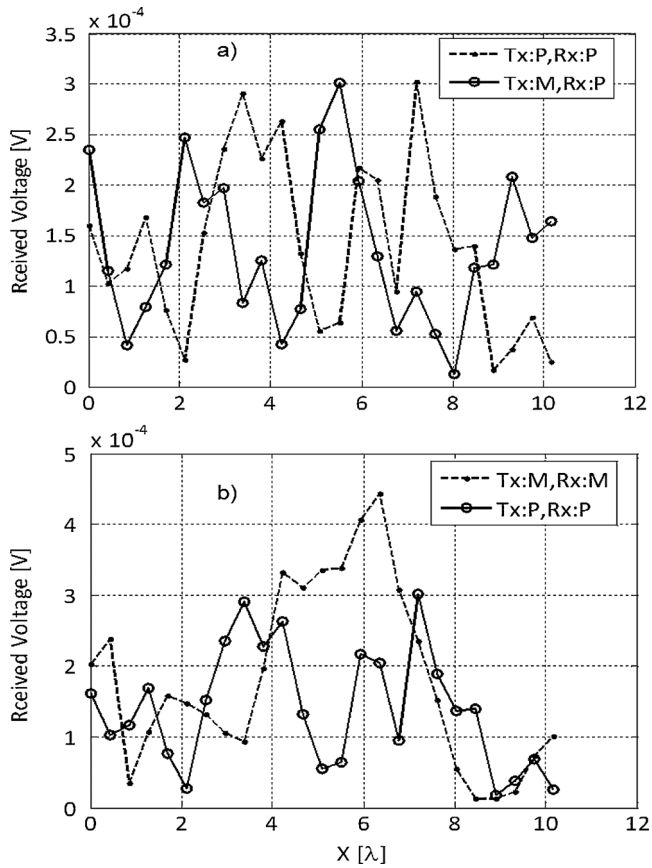

Fig. 16. Measured signals for set up 2 (Fig. 13: (a) received signals from the patch antenna while the patch is transmitting (while the monopole is terminated with 50 Ohm) and when the monopole is transmitting (while the patch is terminated with 50 Ohm), (b) received signal from the monopole when the monopole is transmitting and received signal from patch when the patch is transmitting.

transmitting while the Patch antenna is matched to a 50 Ohm termination are shown in Fig. 15(a) (Case 1). The signals from the other two channels (where Tx is Patch, Case 2) are shown in Fig. 15(b). It is observed that in Case 1 where near-ground wave propagation is excited by the monopole antenna with omnidirectional radiation pattern, the fields radiated by the monopole antenna are well received at both receiving antennas. This is because the use of a finite ground plane makes the radiation pattern of the patch antenna broader, eliminating a desired radiation null at $\theta = 90°$. On the other hand, in Case 2 (Tx is patch), where propagation is mainly supported by rays bouncing between top ceiling and ground are dominantly excited by the patch antenna. The envelop correlation coefficients between the channels for both cases were 0.4 and 0.1 for Case 1 and Case 2, respectively. The variation in the correlation values is due to both the radiation patterns of the antenna elements and the different propagation mechanisms that support the various channels. In both cases, the correlation values are less than 0.5, which meets the required industry standards. This measurement results, in addition to the simulation analysis presented, further validate the feasibility of using the proposed radiation pattern diversity system in rich multi-path indoor environments.

The results of the second and third set of measurements, which correspond to set up 2 and 3 (Fig. 13) are given in Figs. 16 and 17. In all cases, the signals plotted as a function of position demonstrate independently varying magnitudes. These results show the advantage of utilizing the proposed radiation diversity system to create multiple channels with minimal correlation that could be combined to improve channel reliability in multipath environments. The complex correlation values computed for the various pairs of channels in all three scenarios are summarized in Table II. Based on the three set of measurements, the two channels with lowest correlation are: 1) when both Tx and Rx are monopole (M,M) and 2) when both Tx and Rx are patch (P,P). This is because the first channel is mostly supported by near-ground propagation and multiple scattering between sidewalls, while the second channel is mostly supported by rays that bounce between the ground and ceiling. It should be noted that the correlation between other pairs of channels is also low (the maximum correlation value based on these measurements is 0.4 and is as low as 0.1 for some cases). The apparent diversity gain was calculated based the measured results using a selection combining criteria for a 1% outage rate as described in Section II. The apparentdiversity gain for these measurements range from 9.6 dB to 10.4 dB for the cases listed in Table II.

Another way that is often used to demonstrate the performance of diversity systems is based on cumulative distribution functions which are used to describe the output SNR for a given outage rate. In order to analyze the improvement in signal-to-noise ratio as a function of outage rate, a selection combining technique is utilized as described in [19]. Based on

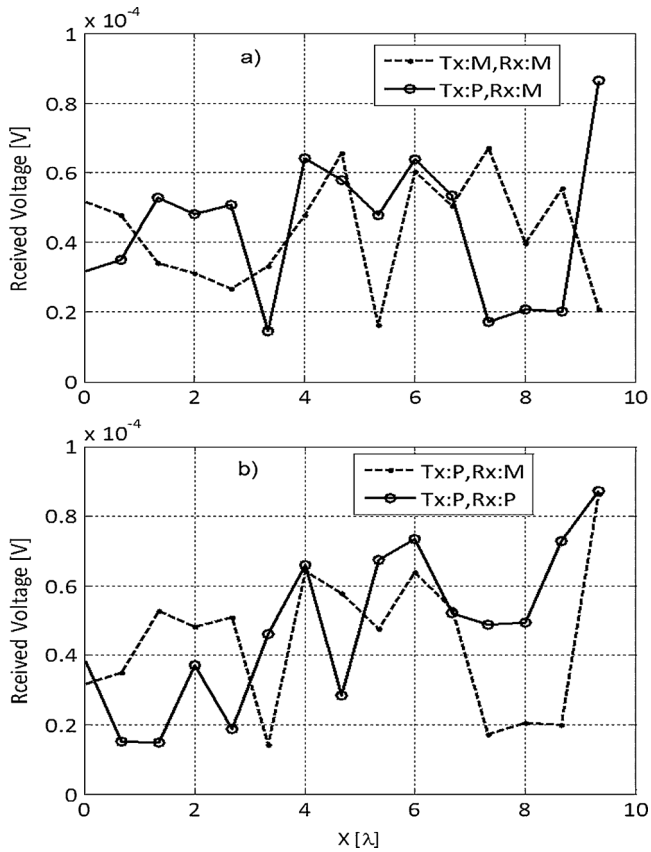

Fig. 17. Measured signals for set up 3 (Fig. 13): (a) received signals from the monopole antenna while the monopole is transmitting (the Tx patch is terminated with 50 Ohm) and when the patch is transmitting (the Tx monopole is terminated with 50 Ohm), (b) when the patch antenna is transmitting while the monopole component of the Tx antenna is terminated with 50 Ohm and the Rx antenna is receiving in both channels.

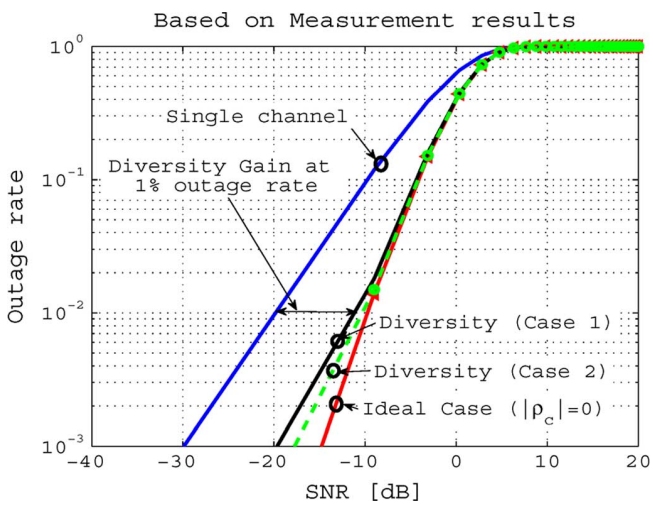

Fig. 18. Output signal-to-noise ratio plotted as a function of the outage rate for a single channel and a two element diversity (i.e., ideal case, measured results using the proposed pattern diversity system). The two channels considered in Case 1 are (P,M) and (P,P). In Case 2, (M,M) and (P,P) are considered. In both cases, the channels are combined based on selection combining. Also, Case 1 and 2 shown above use the measurements results for set up 1 and set up 2, respectively (see Fig. 13).

selection combining, the probability that the instantaneous combiner output SNR γ is below some value x can be calculated (by

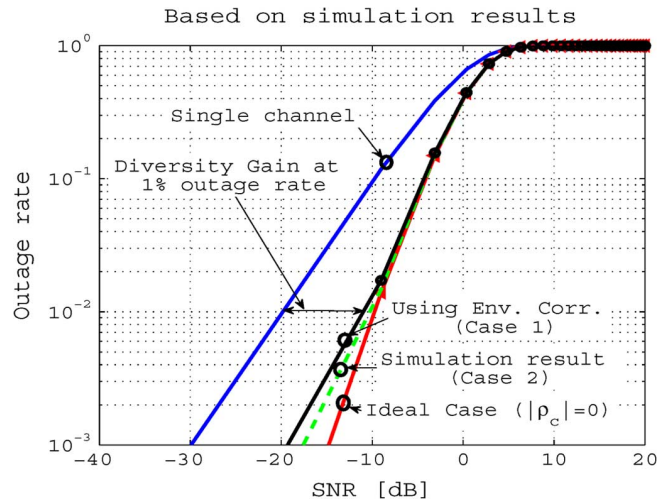

Fig. 19. Output signal-to-noise ratio plotted as a function of the outage rate for a single channel and a two element diversity (i.e., ideal case ($\rho_c = 0$), based on simulation results as given in Table I and based on envelop correlation using (9)). The two channels considered in Case 1 are (M,P) and (M,M). In Case 2, the channels (M,M) and (P,P) are considered. In both cases, the channels are combined based on selection combining.

TABLE I
CORRELATION COEFFICIENTS CALCULATED FOR VARIOUS CHANNELS BASED ON SIMULATION RESULTS ROUNDED TO 1 DECIMAL PLACE (FIG. 4, SET UP 1)

Ch1 (Tx,Rx)	Ch2 (Tx,Rx)	ρ_c	$\lvert\rho_c\rvert$
M,P	M,M	0.0 + 0.0i	0.0
P,M	P,P	-0.2 + 0.1i	0.2
M,M	P,P	-0.2 - 0.2i	0.3

considering the correlation coefficient between the two channels) as

$$Prob(\gamma < x) = 1 - 2e^{\frac{-x}{\Gamma}} Q(\sqrt{Cx}, |\rho_c|\sqrt{Cx}) + e^{-Cx} I_o[|\rho_c| Cx] \quad (9)$$

where Γ is the mean SNR (assuming it is the same for both diversity branches) and ρ_c is the correlation coefficient between the two channels. It should be noted that even if the mean SNR is assumed to be the same in the two branches, the instantaneous branch SNR can be different [24]. The functions Q and I_o are given in [19]. Also, C is given in terms of ρ_c and Γ as

$$C = \frac{2}{\Gamma(1 - |\rho_c|^2)}. \quad (10)$$

Based on (9), the output SNR is plotted against the outage rate in Fig. 18. The single channel case and the ideal two element case (when the correlation is zero) are also plotted. It should be noted that the curves in Fig. 18 are plotted in such a way that the output SNR value corresponding to 50% outage rate for the single channel case is 0 dB. The other two curves shown in Fig. 18 are based on measured results using the proposed pattern diversity system. As can be seen, the proposed pattern diversity system results in a diversity gain of 9.4 dB at 1% outage as alluded to earlier. The results shown in Fig. 19, which are based on simulation results as summarized in Table I, also show similar diversity gain results. As alluded to earlier, (9) is accurate only

TABLE II
CORRELATION COEFFICIENTS CALCULATED FOR VARIOUS CHANNELS BASED ON MEASURED RESULTS ROUNDED TO 1 DECIMAL PLACE (FIG. 10)

Ch1 (Tx,Rx)	Ch2 (Tx,Rx)	Set up 1	Set up 2	Set up 3
P,M	P,P	0.1	0.4	0.2
M,M	P,P	0.3	0.1	0.2
M,M	P,M	0.4	0.0	0.3

when each diversity branch has same SNRs. To check the accuracy of this equation for the proposed diversity system, the ADG values (based on selection diversity) were calculated using the approach described in [24] and similar results were found using both approaches.

V. CONCLUSION

In this paper an analysis of the advantages of a new radiation pattern diversity system is presented. With the advent of enabling antenna miniaturization techniques, radiation pattern diversity offers a unique opportunity to achieve compact diversity antenna systems compared to approaches that utilize spatial diversity. An analysis technique that takes into account the complex radiation pattern of the Tx and Rx diversity antennas in conjunction with an accurate physics-based deterministic propagation model for a complex indoor scenario is proposed. The advantage of this approach is that for a diversity system deployed in complex scenarios the performance can be quantified accurately since all the propagation mechanisms are accounted for. The proposed analysis technique utilizes an efficient deterministic near-ground propagation model along with the complex gain of the Tx and Rx antenna systems. The near-ground indoor propagation model accurately captures scattered field components from indoor obstacles while fully taking into account the Norton surface waves that become dominant for near-ground antennas. In addition, a common aperture radiation pattern diversity system is realized and measurements in complex indoor scenarios are carried out to complement the simulation analysis presented. The diversity gain of the proposed diversity system as well as the envelop and complex correlation coefficients between various channels are computed and utilized to quantify the performance of the proposed system.

REFERENCES

[1] A. Khaleghi, "Diversity techniques with parallel dipole antennas: Radiation pattern analysis," *Progr. Electromagn. Res., PIER*, vol. 64, pp. 23–42, 2006.

[2] J. S. Colburn, Y. Rahmat-Samii, M. A. Jensen, and G. J. Pottie, "Evaluation of personal communications dual-antenna handset diversity performance," *IEEE Trans. Veh. Technol.*, vol. 47, pp. 737–744, Aug. 1998.

[3] R. Narayanan, K. Atanassov, V. Stoiljkovic, and G. Kadambi, "Polarization diversity measurements and analysis for antenna configurations at 1800 MHz," *IEEE Trans. Antennas Propag.*, vol. 52, no. 7, pp. 1795–1810, Jul. 2004.

[4] C. B. Dietrich, Jr., K. Dietze, J. R. Nealy, and W. L. Stutzman, "Spatial, polarization, and pattern diversity for wireless handheld terminals," *IEEE Trans. Antennas Propag.*, vol. 49, no. 9, Sept. 2001.

[5] J. Sarrazin, Y. Mah, S. Avrillon, and S. Toutain, "Collocated microstrip antennas for MIMO systems with a low mutual coupling using mode confinement," *IEEE Trans. Antennas Propag.*, vol. 58, no. 2, pp. 589–592, Feb. 2010.

[6] A. M. D. Turkmani, A. A. Arowojolu, P. A. Jefford, and C. J. Kellet, "An experimental evaluation of the performance of two-branch space and polarization diversity schemes at 1800 MHz," *IEEE Trans. Veh. Technol.*, vol. 44, no. 2, pp. 318–326, Mar. 1995.

[7] P. L. Perini and C. L. Holloway, "Angle and space diversity comparisons in different mobile radio environments," *IEEE Trans. Antennas Propag.*, vol. 46, no. 6, pp. 764–775, Jun. 1998.

[8] P. Mattheijssen, M. H. A. J. Herben, G. Dolmans, and L. Leyten, "Antenna-pattern diversity versus space diversity for use at handhelds," *IEEE Trans. Veh. Technol.*, vol. 53, no. 4, pp. 1035–1042, Jul. 2004.

[9] A. Elsherbini and K. Sarabandi, "UWB high-isolation directive coupled-sectorial-loops antenna pair," *IEEE Antennas Wireless Propag. Lett.*, vol. 10, pp. 215–218, 2011.

[10] J. Oh and K. Sarabandi, "Compact, low-profile, common aperture polarization and pattern diversity antennas," *IEEE Trans. Antennas Propag.*, submitted for publication.

[11] D. Liao and K. Sarabandi, "Near-earth wave propagation characteristics of electric dipole in presence of vegetation or snow layer," *IEEE Trans. Antennas Propag.*, vol. 53, no. 11, pp. 3747–3756, Nov. 2005.

[12] F. Dagefu and K. Sarabandi, "Analysis and modeling of near-ground wave propagation in the presence of building walls," *IEEE Trans. Antennas Propag.*, vol. 59, no. 6, pp. 2368–2378, Jun. 2011.

[13] W. K. Toh, Z. N. Chen, X. Qing, and T. S. P. See, "A planar UWB diversity antenna," *IEEE Trans. Antennas Propag.*, vol. 57, no. 11, pp. 3467–3473, Nov. 2009.

[14] K. Wei, Z. Zhang, W. Chen, and Z. Feng, "A novel hybrid-fed patch antenna with pattern diversity," *IEEE Antennas Wireless Propag. Lett.*, vol. 9, pp. 562–565, 2010.

[15] T. A. Milligan, *Modern Antenna Design*. Piscataway, NJ, USA: IEEE Press, 2005.

[16] K. Rosengren and P.-S. Kildal, "Radiation efficiency, correlation, diversity gain and capacity of a six-monopole antenna array for a MIMO system: Theory, simulation and measurement in reverberation chamber," *IEE Proc.-Microw. Antennas Propag.*, vol. 152, no. 1, pp. 7–16, Feb. 2005.

[17] M. Sonkki, E. Antonino-Daviu, M. Ferrando-Bataller, and E. T. Salonen, "Planar wideband polarization diversity antenna for mobile terminals," *IEEE Antennas Wireless Propag.*, vol. 10, pp. 939–942, 2011.

[18] P. Hallbjrner, "The significance of radiation efficiencies when using S-parameters to calculate the received signal correlation from two antennas," *IEEE Antennas Propag. Lett.*, vol. 4, pp. 97–99, 2005.

[19] M. Schwartz, W. R. Bennet, and S. Stein, *Communication Systems and Techniques*. Piscataway, NJ, USA: IEEE Press, 1996.

[20] J. Yang, S. Pivnenko, T. Laitinen, J. Carlsson, and X. Chen, "Measurements of diversity gain and radiation efficiency of the Eleven antenna by using different measurement techniques," presented at the 4th Eur. Conf. Antennas Propag., Apr. 2010.

[21] [Online]. Available: http://www.emagware.com/

[22] S. Blanch, J. Romeu, and I. Corbella, "Exact representation of antenna system diversity performance from input parameter description," *Electron. Lett.*, vol. 39, pp. 705–707, 2003.

[23] T. K. George, N. Lenin, and M. Sreenivasan, "Wide-band dual sleeve antenna," *IEEE Trans. Antennas Propag.*, vol. 54, no. 3, pp. 1034–1037, 2006.

[24] A. F. Molisch, *Wireless Communications*. New York, NY, USA: Wiley-IEEE Press, 2011.

[25] N. Jamaly, P.-S. Kildal, and J. Carlsson, "Compact formulas for diversity gain of two-port antennas," *IEEE Antennas Wireless Propag. Lett.*, vol. 9, pp. 970–973, 2010.

Fikadu T. Dagefu received the B.S. degree in electrical engineering from the University of Texas at Austin in 2007, the M.S. degree in electrical engineering in 2009 and the Ph.D. degree in electrical engineering from The University of Michigan at Ann Arbor in 2012.

He is currently a Postdoctoral Fellow at the US Army Research Laboratory. His research interests include wave propagation modeling, measurements and channel characterization, positioning and localization in GPS-denied environments, and low power HF/VHF communication with miniaturized antennas.

Dr. Dagefu is the recipient of the 2011 MIT Lincoln Laboratory Graduate Fellowship. He is a member of Eta Kappa Nu and Tau Beta Pi honor societies. He was a finalist in the student paper competitions at the IEEE IGARSS international conference in 2009 and 2010.

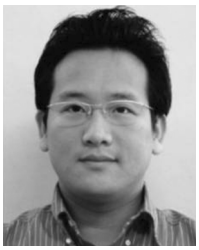

Jungsuek Oh (M'12) received the B.S. and M.S. degrees from Seoul National University, Korea, in 2002 and 2007, respectively, and the Ph.D. degree from the University of Michigan at Ann Arbor in 2012.

From 2007 to 2008, he was with Korea Telecom as a Hardware Research Engineer working on the development of flexible RF devices. In 2012, he was a Postdoctoral Research Fellow with the Radiation Laboratory, the University of Michigan. He is currently a Senior RF Engineer with Samsung Research America—Dallas. His research areas include mmW beam focusing/shaping techniques, antenna miniaturization for integrated systems and radio propagation modeling for indoor scenarios.

Dr. Oh is the recipient of the 2011 Rackham Predoctoral Fellowship Award at the University of Michigan.

Jihun Choi (S'12) received the B.S. degree in electrical engineering from University of Incheon, Korea, in 2010 and the M.S. degree in electrical engineering from The University of Michigan at Ann Arbor in 2013, in which he is currently working toward the Ph.D. degree.

Since 2011 he has been with the Radiation Laboratory, Department of Electrical Engineering and Computer Science, University of Michigan, where he is presently a Graduate Research Assistant.

Kamal Sarabandi (S'87–M'90–SM'92–F'00) received the B.S. degree in electrical engineering from the Sharif University of Technology, Tehran, Iran, in 1980, the M.S. degree in electrical engineering in 1986, and the M.S. degree in mathematics and the Ph.D. degree in electrical engineering from The University of Michigan at Ann Arbor in 1989.

He is currently the Director of the Radiation Laboratory and the Rufus S. Teesdale Professor of Engineering in the Department of Electrical Engineering and Computer Science, The University of Michigan at Ann Arbor. His research areas of interest include microwave and millimeter-wave radar remote sensing, meta-materials, electromagnetic wave propagation, and antenna miniaturization. He possesses 25 years of experience with wave propagation in random media, communication channel modeling, microwave sensors, and radar systems and leads a large research group including two research scientists, 16 Ph.D. students. He has graduated 40 Ph.D. and supervised numerous post-doctoral students. He has served as the Principal Investigator on many projects sponsored by the National Aeronautics and Space Administration (NASA), Jet Propulsion Laboratory (JPL), Army Research Office (ARO), Office of Naval Research (ONR), Army Research Laboratory (ARL), National Science Foundation (NSF), Defense Advanced Research Projects Agency (DARPA), and a large number of industries. Currently he is leading the Center for Microelectronics and Sensors funded by the Army Research Laboratory under the Micro-Autonomous Systems and Technology (MAST) Collaborative Technology Alliance (CTA) program. He has published many book chapters and more than 220 papers in refereed journals on miniaturized and on-chip antennas, meta-materials, electromagnetic scattering, wireless channel modeling, random media modeling, microwave measurement techniques, radar calibration, inverse scattering problems, and microwave sensors. He has also had more than 500 papers and invited presentations in many national and international conferences and symposia on similar subjects.

Dr. Sarabandi served as a member of NASA Advisory Council appointed by the NASA Administrator for two consecutive terms from 2006–2010. He is serving as a vice president of the IEEE Geoscience and Remote Sensing Society (GRSS) and is a member of the Editorial Board of the PROCEEDINGS OF THE IEEE. He was an associate editor of the IEEE TRANSACTIONS ON ANTENNAS AND PROPAGATION and the IEEE SENSORS JOURNAL. He is a member of Commissions F and D of URSI. He was the recipient of the Henry Russel Award from the Regent of The University of Michigan. In 1999 he received a GAAC Distinguished Lecturer Award from the German Federal Ministry for Education, Science, and Technology. He was also a recipient of the 1996 EECS Department Teaching Excellence Award and a 2004 College of Engineering Research Excellence Award. In 2005 he received the IEEE GRSS Distinguished Achievement Award and the University of Michigan Faculty Recognition Award. He also received the best paper Award at the 2006 Army Science Conference. In 2008 he was awarded a Humboldt Research Award from The Alexander von Humboldt Foundation of Germany and received the best paper award at the IEEE Geoscience and Remote Sensing Symposium. He was also awarded the 2010 Distinguished Faculty Achievement Award from the University of Michigan. The IEEE Board of Directors announced him as the recipient of the 2011 IEEE Judith A. Resnik medal. In the past several years, joint papers presented by his students at a number of international symposia (IEEE APS'95,'97,'00,'01,'03,'05,'06,'07; IEEE IGARSS'99,'02,'07;'11 IEEE IMS'01, USNC URSI'04,'05,'06,'10,'11 AMTA'06, URSI GA 2008) have received best paper awards.